

RESEARCH ARTICLE

Compact and low-loss IPD bandpass filter using 3D glass-based redistribution layer technology

HangXing Li | Yazhi Cao  | Peng Zhao | Gaofeng Wang

MOE Engineering Research Center of Smart Microsensors and Microsystems, School of Electronics and Information, Hangzhou Dianzi University, Hangzhou, China

Correspondence

Yazhi Cao, MOE Engineering Research Center of Smart Microsensors and Microsystems, School of Electronics and Information, Hangzhou Dianzi University, Hangzhou, China.
Email: caoyazi@hdu.edu.cn

Funding information

National Natural Science Foundation of China, Grant/Award Numbers: 92373202, 62141409; National Key Research and Development Program of China, Grant/Award Number: 2019YFB2205003; Fundamental Research Funds for the Provincial Universities of Zhejiang, Grant/Award Number: GK239909299001-005

Abstract

A low-loss miniaturized bandpass filter is presented using 3D glass-based RDL packaging technology. A new topology consisting of one modified Pi-section and one modified T-section is introduced to generate three transmission zeros which can achieve the high out-of-band rejection. A combination of 2D planar inductors and high-Q 3D inductors is used to achieve low insertion loss and minimize the filter size. In addition, one grounded resonator at input terminal is introduced to generate an extra transmission zero in the low end. The proposed bandpass filter covering 3.3–4.2 GHz is fabricated with a compact size of 1.6 mm × 0.8 mm × 0.25 mm. It exhibits an insertion loss of less than 1.0 dB at a center frequency of 3.75GHz and a return loss of better than 14 dB. The proposed design has a 3 dB fractional bandwidth of 37.6%. Its out-of-band rejection is better than 20 dB at the low frequency band from DC to 2.0 GHz and better than 19 dB at the high frequency band from 5.0 to 9.0 GHz. The simulated and measured results of the proposed BPF are in reasonably good agreement.

KEYWORDS

band pass filter (BPF), low insertion loss, redistribution layer (RDL), transmission zero

1 | INTRODUCTION

To satisfy the ever-increasing requirements of emerging wireless communication systems, advanced RF/microwave passive devices are needed.¹ Specifically, bandpass filters (BPFs) with compact size, low insertion loss and high out-of-band rejection have become critical for radio frequency (RF) front-end modules.^{2,3}

In low temperature co-fired ceramics (LTCC) technology, there are some effective methods to enhance the out-of-band rejection of a bandpass filter by adding transmission zeros (TZs). A design based on a novel compact 3D dual-mode step impedance resonator (SIR) was proposed.⁴ Moreover, the controllable transmission zeros can be also generated by stepped-impedance stubs (SISs) to obtain high selectivity.⁵ In addition, a LTCC broadband bandpass filter using coupling lines with open/short-circuit stubs was also reported.⁶ However, the LTCC filter has low process consistency and usually a large size.

Integrated passive device (IPD) technology adopts wafer manufacturing process and has merits of small size, low cost, high consistency, and high integration level.^{7–16} Source-load coupling was introduced to produce an additional pair of transmission zeros located on both sides of the passband and a Pi-section circuit was designed to obtain TZ at the upper sideband.^{8,10,16} Controllable filter circuit was introduced to improve out-of-band rejection and extend the

upper stopband.^{9,12} A compact and high-order on-chip wideband BPF on stepped-impedance MMR was presented on GaAs-based IPD technology.¹³ However, the insertion loss of the above designs is not particularly favorable.

In this work, a compact IPD bandpass filter is designed using 3D glass-based RDL (Redistribution Layer) packaging technology to overcome the issues mentioned above. It introduces a new topology based on the cascade of the modified T-section topology and the modified Pi-section topology. In order to improve out-of-band rejection and selectivity at low frequencies, one grounded resonator consisting of the inductor and capacitor connected in series to ground is introduced to generate one extra transmission zero in the low end. The proposed bandpass filter is fabricated and measured. It can achieve a compact size of $1.6 \text{ mm} \times 0.8 \text{ mm} \times 0.25 \text{ mm}$, an insertion loss less than 1.0 dB at the center frequency and a return loss better than 14 dB. The proposed BPF can achieve a competitive performance compared with the existing works.

2 | DESIGN AND ANALYSIS

2.1 | Proposed BPF topology

As shown in Figure 1A, the proposed bandpass filter consists of a modified T-section (structure A), a modified Pi-section (structure B), and a grounded resonator (structure C). The modified T-section with high-pass characteristic as

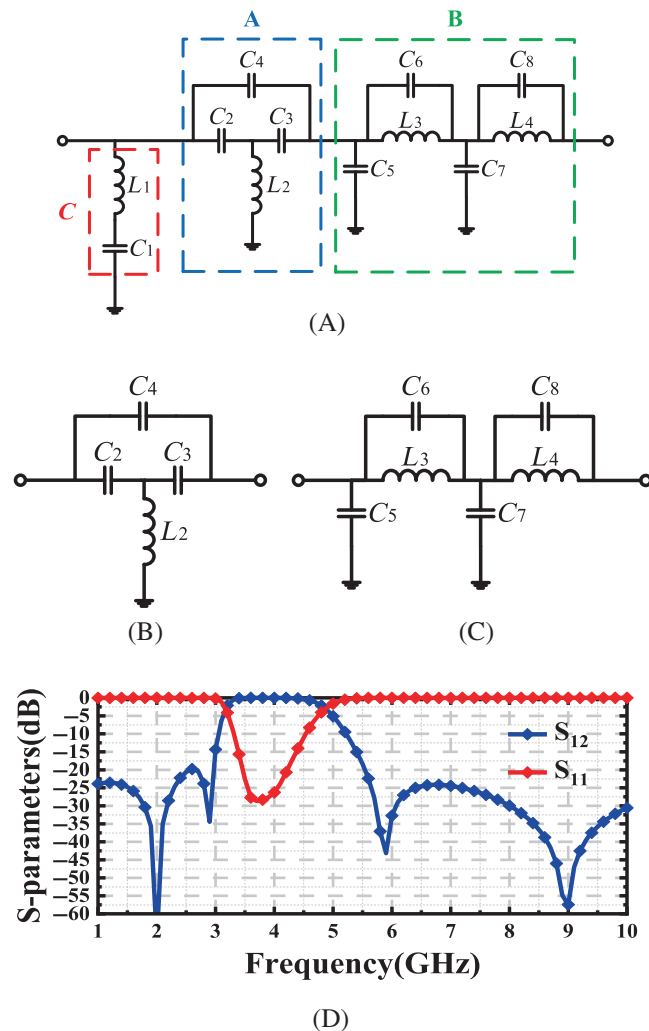


FIGURE 1 (A) The schematic of proposed BPF. (B) Proposed lumped T-section. (C) Proposed lumped Pi-section. (D) Simulated results of the lumped BPF. The elements of the proposed lumped BPF are as follows: $C_1 = 0.402 \text{ pF}$, $C_2 = 0.384 \text{ pF}$, $C_3 = 0.528 \text{ pF}$, $C_4 = 0.131 \text{ pF}$, $C_5 = 0.318 \text{ pF}$, $C_6 = 0.507 \text{ pF}$, $C_7 = 0.870 \text{ pF}$, $C_8 = 0.226 \text{ pF}$; $L_1 = 7.580 \text{ nH}$, $L_2 = 2.568 \text{ nH}$, $L_3 = 1.453 \text{ nH}$, and $L_4 = 1.397 \text{ nH}$.

shown in Figure 1B, is introduced to achieve high out-band rejection at the low frequency range. In this modified T-section topology, a source-load coupling capacitor C_4 is connected at both ends of the traditional T-section. It can generate an extra TZ at low end and improve out of band rejection at this low end.

This modified T-section circuit can be equated to two subnetworks. As in Figure 1B, where y'_{11} , y'_{12} , y'_{21} , and y'_{22} are the parameters of the admittance matrix of the traditional T-section. Thus, the admittance matrix of the modified T-section circuit is:

$$Y = \begin{bmatrix} j\omega C_4 + y'_{11} & -j\omega C_4 + y'_{12} \\ -j\omega C_4 + y'_{21} & j\omega C_4 + y'_{22} \end{bmatrix}, \quad (1)$$

where ω is the angular frequency. The corresponding S parameters can be obtained as with the following equation:

$$S_{12} = \frac{-2Y_{12}Y_0}{\Delta Y}, \quad (2)$$

$$S_{21} = \frac{-2Y_{21}Y_0}{\Delta Y}. \quad (3)$$

Once the frequency of $S_{12} = S_{21} = 0$ is determined, the finite transmission zero frequency position is:

$$Y_{12} = Y_{21} = -j\omega C_4 + y'_{12} = -j\omega C_4 + y'_{21} = 0. \quad (4)$$

The ABCD matrix of the traditional T-section is expressed as:

$$\begin{bmatrix} A & B \\ C & D \end{bmatrix} = \begin{bmatrix} 1 & -j\frac{1}{\omega C_2} \\ 0 & 1 \end{bmatrix} \begin{bmatrix} 1 & 0 \\ -j\frac{1}{\omega L_2} & 1 \end{bmatrix} \begin{bmatrix} 1 & -j\frac{1}{\omega C_3} \\ 0 & 1 \end{bmatrix} = \begin{bmatrix} 1 - \frac{1}{\omega^2 L_2 C_2} & j\frac{1 - \omega^2 L_2 C_2 - \omega^2 L_2 C_3}{\omega^3 L_2 C_2 C_3} \\ -j\frac{1}{\omega L_2} & 1 - \frac{1}{\omega^2 L_2 C_3} \end{bmatrix}. \quad (5)$$

According to Equation (4), the location of the transmission zero in the filter can be calculated as:

$$y'_{12} = y'_{21} = -\frac{1}{B} = j\frac{\omega^3 L_2 C_2 C_3}{1 - \omega^2 L_2 C_2 - \omega^2 L_2 C_3} = j\omega C_4, \quad (6)$$

$$f_1 = \frac{\omega_1}{2\pi} = \frac{1}{2\pi} \sqrt{\frac{C_4}{L_2(C_2 C_3 + C_2 C_4 + C_3 C_4)}}. \quad (7)$$

Herein, it is assumed that $C_2 = 0.384$ pF, $C_3 = 0.528$ pF, $C_4 = 0.131$ pF, and $L_2 = 2.568$ nH. The TZ frequency is then obtained as $f_1 = 2.02$ GHz. As shown in Figure 2B, the TZ position moves from 2.3 to 1.8 GHz when the value of capacitor C_2 is increased from 0.1 to 0.2 pF. By increasing the value of C_2 can enhance the out-of-band rejection at lower frequencies and attenuates the out-of-band rejection at higher frequencies.

The modified Pi-section with low-pass characteristic as shown in Figure 1C, is introduced to achieve high out-band rejection at the high frequency range. In this modified topology, C_6 and C_8 are connected in parallel with L_3 and L_4 , respectively. It can generate two TZs at the high end and improve out of band rejection at this high end.

In order to analyze the modified Pi-section circuit, the ABCD matrix of the two-port network can be written as:

$$\begin{bmatrix} A & B \\ C & D \end{bmatrix} = \begin{bmatrix} 1 & 0 \\ j\omega C_5 & 1 \end{bmatrix} \begin{bmatrix} 1 & jZ_1 \\ 0 & 1 \end{bmatrix} \begin{bmatrix} 1 & 0 \\ j\omega C_7 & 1 \end{bmatrix} \begin{bmatrix} 1 & jZ_2 \\ 0 & 1 \end{bmatrix} = \begin{bmatrix} 1 - \omega C_7 Z_1 & jZ_1 + jZ_2 - j\omega C_7 Z_1 Z_2 \\ j\omega C_5 + j\omega C_7 - j\omega^2 C_5 C_7 Z_1 & 1 + \omega^2 C_5 C_7 Z_1 Z_2 - \omega C_5 Z_1 - \omega C_5 Z_2 - \omega C_7 Z_2 \end{bmatrix}, \quad (8)$$

where $Z_1 = \frac{1-\omega^2 L_3 C_6}{j\omega L_3}$, $Z_2 = \frac{1-\omega^2 L_4 C_8}{j\omega L_4}$, where ω is the angular frequency. The corresponding S parameters can be obtained as with the following equation:

$$S_{12} = \frac{2(AD - BC)}{A + B/Z_0 + CZ_0 + D}, \quad (9)$$

According to (8) and (9), the TZ frequencies f_2 and f_3 can be calculated as

$$f_2 = \frac{\omega_2}{2\pi} = \frac{1}{2\pi} \sqrt{\frac{1}{L_3 C_6}}, f_3 = \frac{\omega_3}{2\pi} = \frac{1}{2\pi} \sqrt{\frac{1}{L_4 C_8}}. \quad (10)$$

Herein, it is assumed that $C_6 = 0.507$ pF, $C_8 = 0.226$ nH; $L_3 = 1.453$ nH, and $L_4 = 1.397$ nH. The two TZ frequencies are obtained as $f_2 = 5.864$ GHz and $f_3 = 8.957$ GHz, respectively.

In addition, in order to improve the out-of-band suppression of the lower stopband and also improve the impedance match in the passband, L_1 and C_1 are connected in series to the ground at the input terminal. This newly added structure can generate an extra transmission zero at 2.88 GHz (where it is assumed that $L_1 = 7.580$ nH and $C_1 = 0.384$ pF), thereby improving out-of-band suppression at the low frequency end from 2 to 3 GHz. As shown in Figure 2A, the TZ position can be moved from 3.3 to 2.6 GHz when the value of capacitor C_1 is increased from 0.3 to 0.5 pF. Increasing the value of C_1 moves this transmission zero to a lower frequency position to further increase the suppression level. However as shown in Figure 2A, in order to obtain a better roll off coefficient, this transmission zero of the low frequency are designed closer to the passband.

2.2 | High-Q 3D glassed-based inductor

The cross-sectional view of the 3D packaging technology is composed of RDL and glass substrate as shown in Figure 3. This RDL consists of two metal layers M1 and M2. As shown in Figure 4A, a 2D planar inductor with 2.5 turns is

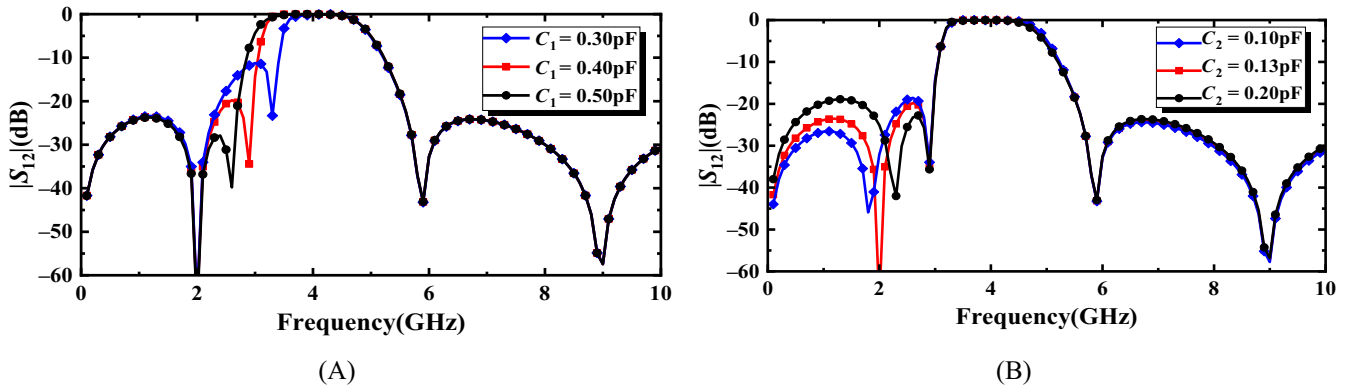


FIGURE 2 (A) Simulated frequency response curves of the lumped BPF with changed values C_1 . (B) The lumped BPF Simulated frequency response curves of the lumped BPF with changed values C_2 .

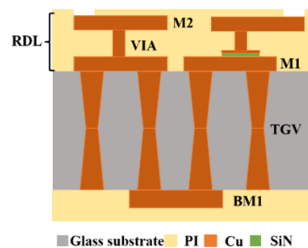


FIGURE 3 Cross-sectional view of the 3D glass-based RDL packaging technology.

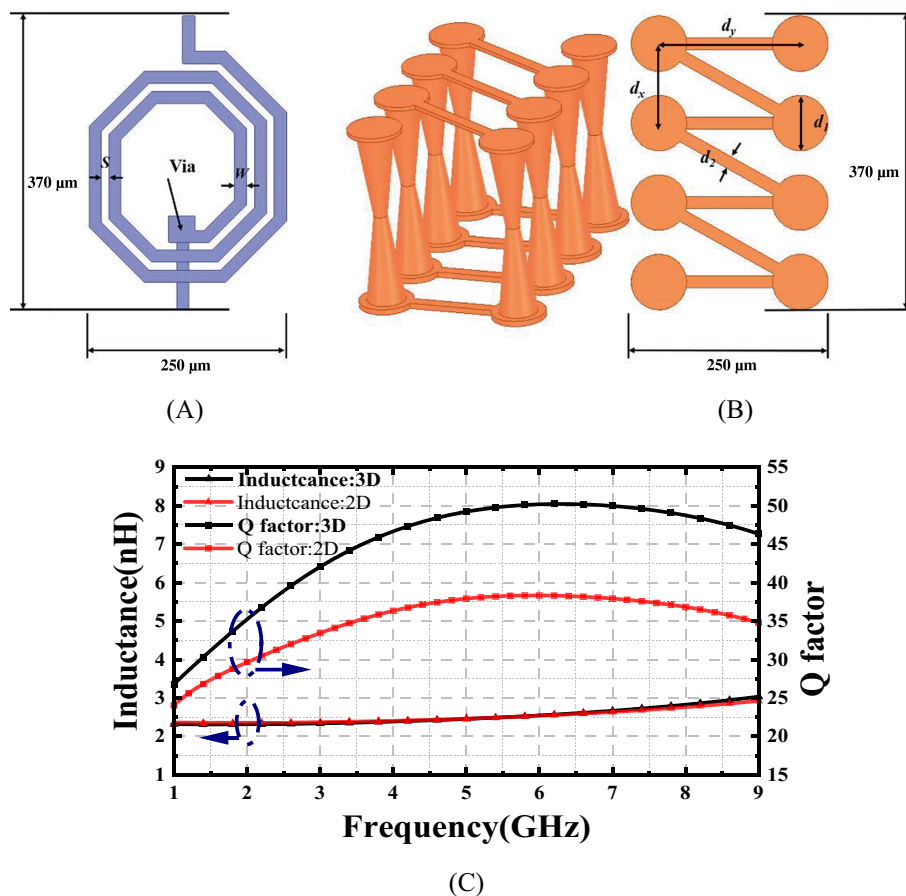


FIGURE 4 (A) Planar 2D inductor structure (Dimensions: $W = 15$, $S = 10$ unit: μm). (B) 3D inductor structure. (Dimensions: $d_x = 100$, $d_y = 178$, $d_1 = 70$, $d_2 = 15$ unit: μm). (C) Comparison of simulated inductance and Q factor between the planar 2D inductor structure and 3D inductor structure.

designed on RDL. On the other hand, a 3D inductor with higher Q factor is used to improve the selectivity near the filter passband. This 3D inductor with four turns consists of three parts on M1, BM1 and TGV, respectively, as shown in Figure 4B.

The simulated inductances and Q factors of the 2D planar inductor and the high-Q 3D inductor with the similar dimension of $370 \mu\text{m} \times 250 \mu\text{m}$ is compared in Figure 4C. It shows that the Q factor of this 3D inductor is 21%–58% higher than that of the 2D planar inductor, while the inductances of both inductors are similar. Therefore, using high-Q 3D inductor can reduce the insertion loss of the designed filter. Since the 2D planar inductor and the 3D inductor are not located on the same metal layer, they can be realized one on top of the other, and thus a mixed use of 2D planar inductor and high-Q 3D inductor can make the filter design more compact.

3 | FABRICATION AND MEASUREMENT

The proposed IPD BPF design is fabricated using the 3D RDL-based packaging technology on glass substrate. The glass substrate has thickness of $230 \mu\text{m}$, a relative dielectric constant ϵ_r of 4.4, and the loss tangent $\tan\delta$ is 0.0073. Resistive losses will have an effect on the S-parameter performance like insertion loss and attenuation, but not the transmission zero position. It provides three metal layers (Cu) including M1, M2, and BM1 with thicknesses of 5, 5, and $7 \mu\text{m}$, respectively. The MIM capacitors are fabricated on the M1 and M2 layers, which are separated by a dielectric layer of a relative dielectric constant ϵ_r of 6.8.

The proposed filter layout is shown in Figure 5A, in which L_1 , L_2 , and L_4 are implemented as planar 2D inductors, and L_3 is implemented as a 3D inductor. The high-frequency TZ near the passband is generated by the resonator composed of L_3 and C_6 . Moreover, a mixed use of 2D planar inductor and high-Q 3D inductor is adopted to reduce the size

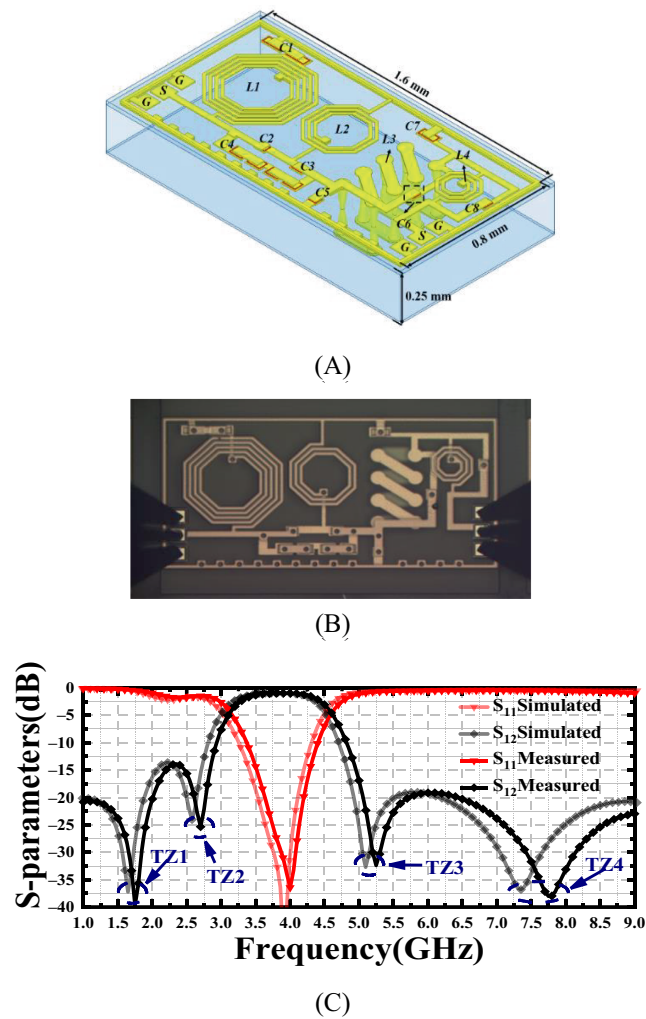


FIGURE 5 (A) Chip layout 3D view. (B) Micrograph of the proposed BPF. (C) Simulated and measured results of the proposed BPF.

and the insertion loss. Note that increasing the Q factor of L_3 can improve the selectivity of the passband and reduce the insertion loss.

The GDS layout of the proposed filter is generated by the full-wave electromagnetic simulator, UltraEM, from Faraday Dynamics.¹⁷ The micrograph of the proposed BPF design is shown in Figure 5B, respectively. The layout size of the fabricated BPF chip is $1.6 \text{ mm} \times 0.8 \text{ mm} \times 0.25 \text{ mm}$. The electrical size of the filter can be calculated as $0.042 \lambda_g \times 0.021 \lambda_g$.

The fabricated BPF is measured on-chip using the Keysight N5244A PNA-X vector network analyzer and Cascade summit-11 000 probe station. We applied the SOLT de-embedding method during the measurement process, which is based on a 12-item error model and can reduce the impact of system errors on the measurement results. The simulated and measurement results of the proposed BPF are compared in Figure 5C. The simulation results are in good agreement with the measured ones. From the measurement results, the insertion loss at the center frequency of 3.75 GHz is less than 1.0 dB, the return loss is better than 14 dB and the measured BPF with a 3-dB fractional bandwidth (FBW) of 37.6%. The measured results show that its out-of-band rejection is better than 20 dB at the low frequency band from DC to 2.0 GHz and better than 19 dB at the high frequency band from 5.0 to 9.0 GHz. There are some slight frequency offsets between the simulation results and the measurement results, due to the processing error of the dielectric constant of the capacitor layer SiN.

Table 1 summarizes the performance of the designed BPF. It is observed that the insertion loss performance of the proposed BPF is much better in comparison with other prior designs except.¹⁵ The proposed BPF can achieve a more compact size compared with those from.^{5,6,9,14,15} Moreover, this proposed filter exhibits more TZs compared

TABLE 1 Comparison of the proposed BPF with several reported BPF.

Ref.	f_0 (GHz)	Insertion loss (dB)	Size (λ_0^2) $\times 10^{-4}$	Return loss (dB)	TZs	19-dB rejection	Process
5	3.50	1.35	7×8	12.8	5	$2.2 f_0$	LTCC
6	3.03	2.00	9.8×7.9	15	4	$2.9 f_0$	LTCC
7	3.75	1.50	1.3×0.9	16	5	$8.3 f_0$	HRS
16	2.45	2.60	1.13×0.69	15	3	$5.7 f_0$	HRS
9	3.43	2.73	2.7×1.5	17	2	$2.9 f_0$	GaAs
10	3.35	2.05	1.675×0.67	19	3	$12 f_0$	GaAs
14	8.60	2.10	23.36×11.63	10	1	$1.6 f_0$	Glass
15	4.20	0.96	3.4×2.6	20	3	$1.9 f_0$	Glass
This work	3.75	1.00	2×1	14	4	$2.4 f_0$	Glass

Note: λ_0 , the wavelength in air at f_0 ; TZs, transmission zeros near the passband.

with,^{9,10,14–16} thereby significantly improve the high suppression in the wide upper stopband. The proposed BPF is suitable for integrating with 5G radio frequency front-end systems.

4 | CONCLUSIONS

In this work, a miniaturized BPF design with low insertion loss has been presented and fabricated using the 3D glass-based RDL packaging technology. A new topology consisting of a modified Pi-section cascaded with a T-section was introduced to generate three transmission zeros and can achieve the high suppression in the wide upper stopband. A combination of 2D planar inductors and high-Q 3D inductors has been utilized to reduce insertion loss and achieve chip miniaturization. In addition, connecting the inductor and capacitor in series to the ground can generate one extra transmission zero in the low end. The proposed BPF has been measured by on-wafer probing with GSG probes. The measurement results are in accordance with the simulated results. The filter has a bandwidth range of 3.3–4.2 GHz. It has an insertion loss of less than 1.0 dB at the center frequency and a return loss of better than 14 dB. The size of the fabricated BPF is miniaturized to $1.6 \text{ mm} \times 0.8 \text{ mm} \times 0.25 \text{ mm}$, which is suitable for 5G RF frontend system integrated circuits.

ACKNOWLEDGMENTS

This work was supported by National Natural Science Foundation of China under Grant 92373202, 62141409, Fundamental Research Funds for Provincial Universities of Zhejiang under Grant GK239909299001-005, National Key Research and Development Program of China under Grant 2019YFB2205003.

DATA AVAILABILITY STATEMENT

Data sharing not applicable to this article as no datasets were generated or analysed during the current study.

ORCID

Yazi Cao  <https://orcid.org/0000-0001-6636-3662>

REFERENCES

- Zhao X-B, Wei F, Zhang PF, Shi XW. Mixed-mode magic-Ts and their applications on the designs of dual-band balanced out-of-phase filtering power dividers. *IEEE Trans. Microw. Theory Techn.* 2023;71(9):3896-3905.
- Shi Z-H, Wei F, Yang L, Gómez-García R. High-selectivity inverted microstrip gap waveguide bandpass filter using hybrid cavity and stub-loaded ring resonant modes. *IEEE Trans. Circuits Syst. II Express Briefs.* 2024;71(1):146-150.
- Ma H, Hu Z, Yu D. A low-loss bandpass filter with stacked double-layer structure using glass-based integrated passive device technology. *IEEE Electron Device Lett.* 2023;44(7):1216-1219.
- Chen J-X, Zhan Y, Xue Q. Novel LTCC distributed-element wideband bandpass filter based on the dual-mode stepped-impedance resonator. *IEEE Trans Compon Packag Manuf Technol.* 2015;5(3):372-380.

5. Zhao W, Wu Y, Yang Y, Wang W. LTCC bandpass filter chips with controllable transmission zeros and bandwidths using stepped-impedance stubs. *IEEE Trans Circuits Syst II Express Briefs*. 2022;69(4):2071-2075.
6. Feng W, Gao X, Che W, Yang W, Xue Q. LTCC wideband bandpass filters with high performance using coupled lines with open/shorted stubs. *IEEE Trans Compon Packag Manuf Technol*. 2017;7(4):602-609.
7. Zhang J, Xu J-X, Yao C, Zhang XY. Miniaturized high-selectivity high-resistivity-silicon IPD bandpass filter based on multiple transmission paths. *IEEE Electron Device Lett*. 2024;45(4):534-537.
8. Zhang Q, Cao Y, Wang G. Miniaturized IPD band pass filter with low insertion loss based on modified T-section for 5G applications. *Int J Numer Model*. 2024;37(3):e3248.
9. Xu Y, Wu Y, Wu H, Yang Y, Wang W. Wideband high selectivity filter chips with adjustable bandwidth based on IPD technology. *IEEE Trans Circuits Syst II Express Briefs*. 2022;69(11):4273-4277.
10. Luo X-H, Cheng X, Zhang L, et al. A miniaturized on-chip BPF with ultrawide stopband based on lumped Pi-section and source-load coupling. *IEEE Microw. Wirel. Compon. Lett*. 2019;29(8):516-519.
11. Lyu Y-P, Zhou Y-J, Zhu L, Cheng C-H. Compact and high-order on-chip wideband bandpass filters on multimode resonator in integrated passive device technology. *IEEE Electron Device Lett*. 2022;43(2):196-199.
12. Jiang Y, Feng L, Zhu H, et al. Bandpass filter with ultra-wide upper stopband on GaAs IPD technology. *IEEE Trans Circuits Syst II Express Briefs*. 2022;69(2):389-393.
13. Yu H, Wu Y, Yang Y, Wang W. IPD millimeter-wave bandpass filter chip based on stepped-impedance coupled-line dual-mode resonator for 5G application. *IEEE Trans Circuits Syst II Express Briefs*. 2022;69(12):4744-4748.
14. Zhang W, Gu J, Li L, Li X. Through-glass-via based microstrip band-pass filters fabricated with wafer-level low-melting-point alloy micro-casting. *IEEE Electron Device Lett*. 2020;41(7):1106-1109.
15. Li W, Zhang J, Gao L, et al. Compact TGV-based bandpass filters using integrated dual composite right/left-handed resonators. *IEEE Trans Circuits Syst II Express Briefs*. 2024;71(4):1939-1943.
16. Qi Y, Cao Y, Yuan B, Chen S, Wang G. Miniaturized IPD bandpass filter with controllable transmission zero based on modified lumped T-section. *Microw Opt Technol Lett*. 2024;66:e34134.
17. Faraday Dynamics. *Data sheet-IPD. UltraEM V2022*. Faraday Dynamics, Inc.; 2022.

How to cite this article: Li H, Cao Y, Zhao P, Wang G. Compact and low-loss IPD bandpass filter using 3D glass-based redistribution layer technology. *Int J Numer Model*. 2024;37(5):e3292. doi:[10.1002/jnm.3292](https://doi.org/10.1002/jnm.3292)